Electrical and Raman scattering studies of ZnO:P and ZnO:Sb thin films

J. Ayres de Campos[a], T. Viseu[a], A. G. Rolo[a], N.P. Barradas[b], E. Alves[b] T. de Lacerda-Arôso[a], M.F. Cerqueira[a,*]

[a] *Departamento de Física, Universidade do Minho, Campus de Gualtar 4710-057 Braga, Portugal*

[b] *Instituto Tecnológico Nuclear ITN, EN 10, 2686-953 Sacavém, Portugal*

* Correspondence to: M.F. Cerqueira, Centro de Física, Universidade do Minho, Campus de Gualtar, 4710-057 Braga, Portugal. Tel: +351 253 604332, Fax: +351 253 604061, Email: fcerqueira@fisica.uminho.pt

Abstract

A study on the structure, electrical and optical properties of ZnO thin films produced by r.f. magnetron sputtering and implanted either with phosphorous (P) or antimony (Sb) is reported in this work. Raman spectroscopy, X-ray diffraction, optical transmittance and Hall effect measurements have been employed to characterize the samples. X-ray diffraction and Raman scattering patterns confirm that, after a 500ºC annealing, the doped films keep a polycrystalline nature with (002) preferred orientation. These films are very transparent and Hall effect results show that all have p-type conduction, despite doping ion and dose. The electric resistivity reaches values of 0.012 (Ωcm) and 0.042 (Ωcm) for the P and Sb-doped samples, respectively.

Keywords: ZnO; Ion implantation; p-type doping; X-ray; Raman; Hall effect.

1. Introduction

Zinc oxide (ZnO) is a II–VI wide direct-gap semiconductor with a band gap of 3.37 eV at room temperature and a free exciton energy of $\approx$ 60 meV. Both characteristics make it an

interesting material for optoelectronic applications in the near ultraviolet (UV) region, such as UV light-emitting diodes and diode lasers [1,2]. ZnO-derived materials have other potential technological applications, namely as transparent conductive contact, as alternative to ITO [3,4]. A wider field of applications will be reached as soon as a stable and reproducible p-doped ZnO is processed [5]. However ZnO is an intrinsic n-type semiconductor due to its natural defects - oxygen vacancies or interstitial zinc. Thus, **it is** difficult to produce p-type doped-ZnO, achieving low electrical resistivity and high-hole concentration, because of its self-compensating effect, deep acceptor level, and low solubility of acceptor dopants.

In this work, a study on the optical and electrical properties of ZnO thin films doped either by phosphorous (P) or antimony (Sb) is presented. Crystalline structure and optical and electrical properties have been analyzed as a function of the doping species and of it concentration.

2. Experimental

Transparent ZnO thin films have been produced by r.f. magnetron sputtering method [6], in an Alcatel SCM 650 sputtering system. Radio frequency (13.56 MHz) reactive sputter deposition has been carried out (RF power of 50W) after the camera had reached a base pressure of 5×10^{-5} Pa. The target consisted of a hyper-pure (99.99%) metal zinc wafer spaced 60 mm away from the substrates and the deposition has been performed under a mixture of O_2 and Ar gases. The produced films have thickness of about 250 nm. After ZnO deposition, the samples have been separated in two series, implanted either with phosphorous (P) or with antimony (Sb). Doping nominal doses have been 1×10^{15} (ZnO:P1, ZnO:Sb1), 5×10^{15} (ZnO:P2, ZnO:Sb2) and 10×10^{15} atoms cm^{-2} (ZnO:P3,

ZnO:Sb3). The implantation energy has been 50 KeV for Sb and 100 KeV for P. Afterwards, the films have been annealed in vacuum for one hour at 500°C, in order to recover from the implantation damage and to activate the implanted ions. Structural and electrical characterisation of the doped samples has been entirely performed after this thermal treatment.

X-ray diffraction and Raman spectroscopy have been used in order to characterize the films microstructure. X-ray experiments have been performed at room temperature in a Philips PW 1710 diffractometer using Cu-K$_{\alpha}$ radiation, in a Bragg-Bretano geometry in the range $30^{\circ} < 2\theta < 41^{\circ}$. Micro-Raman spectra have been measured in a frequency range of 200-2000 cm^{-1}, using the 514.5 and the 488 nm excitation lines of an Ar^{+} laser, in the back scattering geometry, on a Jobin-Yvon T64000 spectrometer equipped with a liquid nitrogen-cooled CCD detector. The incident laser power has been kept at 9 mW and each scan has been acquired at room temperature for over 600s (60s/scan). Each scan has been repeated at least once to ensure the reproducibility of data.

In order to check the incorporation of doping ions into the ZnO matrix, XPS measurements have also been carried out in a few samples, under monochromatic Al-K$_{\alpha}$ radiation (h$\nu = 1486.92$ eV) using a VG Escalab 250 iXL ESCA instrument (VG Scientific).

Optical transmittance spectra of the films have been assessed by means of a Shimadzu UV 3101 PC spectrophotometer. Thickness and optical parameters in the visible and near infrared range (from 250 to 2500 nm) have been obtained from these spectra by the Minkov method [7]. The dispersion of the dielectric constant used in the parameterization

of the optical constants of the films is based on a classical Lorentz/Drude dielectric function, $\widetilde{\varepsilon}(E)$:

$$\widetilde{\varepsilon}(E) = \varepsilon_\infty + \frac{fE_0^2}{E_0^2 - E^2 + i\gamma_b E} - \frac{C}{E^2 + i\gamma_f E}$$

where ε_∞ is the high frequency dielectric constant, E_0, γ_b and f are, respectively, the resonance energy frequency, the line-width and the strength of the Lorentzian oscillator, related with the bound electrons,. C is a constant associated to the number of free carriers and γ_f is the corresponding dumping related to the inverse of the mobility.

Electric resistivity has been measured at room temperature in a standard d.c. system by using the Van der Pauw technique [8]. Hall-effect measurements have been carried out under the same four-point configuration in a magnetic field of 1300mT, using both polarities of current and magnetic field.

3. Results and discussion

Figure 1 depicts transmittance spectra of a typical ZnO film before implantation (as grown), immediately after implanting phosphorous (heavier dose) and after thermal annealing. Films remained very transparent in the visible and near IR range and with good optical quality, exhibiting well defined transmittance fringes. In inset, a detail of the fitting to data. Damage created by ion implantation into the ZnO films as well as the recovering from it by thermal treatment are well perceptible on these spectra.

XPS analysis performed in one P-doped sample (ZnO:P2) reveals that it is stequiometric and contains both P-O and Zn-O bonds but no P-Zn, enabling to state that most of the dopant ions are in substitutional Zinc sites.
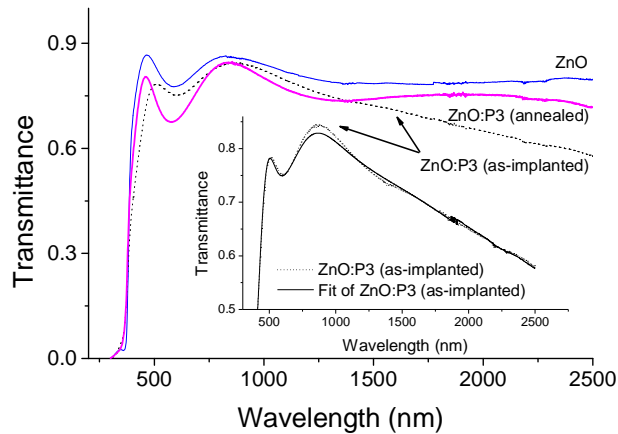
Figure 1 – Transmittance spectra of an as-grown ZnO thin film and of the same film implanted with phosphorous, before and after annealing. The inset shows a typical fit that allows determining thickness and optical parameters.

All the as-grown ZnO thin films show single phase hexagonal wurtzite structure with highly crystalline preferential orientation along the c-axis, perpendicular to the substrate surface. These films present such high electrical resistivity that we have not been able to measure it by the traditional four-point method. The well oriented hexagonal, wurtzite structure is maintained in doped samples, as confirmed by X-ray diffraction spectra.

The c-lattice parameter domain size (D), in addition to the strain along c-axis (e_{zz}), and the corresponding stress (σ) have been calculated according to common procedure described in the literature [9,10]. Data in Table I reveal that the annealing treatment releases completely the compressive stress in doped samples. However, the average domain size in all doped samples is smaller than in the non-doped ones submitted to the same annealing treatment, indicating that the crystalline damage due to implantation has not entirely been recovered. This effect is even clearer in P-doped samples.

Table I - Structural parameters obtained by XRD of undoped and doped ZnO thin films. D stands for the domain size and σ for the stress along c-axis.

sample	2θ (200) (degree)	D (nm)	σ (GPa)
ZnO - as grown	33.76	6.2	-8.5
ZnO - annealed	34.34	25.7	-1.0
ZnO - P1	34.44	15.1	0.2
ZnO - P3	34.39	13.0	-0.5
ZnO - Sb1	34.41	20.2	-0.1
ZnO - Sb3	34.44	16.9	0.2

Results of the electrical resistivity (ρ) of doped samples obtained through a Van der Pauw geometry, of their carrier concentration (n_{Hall}) and Hall mobility (μ_{Hall}) calculated from Hall effect measurements [11] are shown in Table II. Resistivity values as low as 0.012 Ωcm and 0.042 Ωcm have been obtained for P and Sb-doping respectively. All the annealed-doped films present p-type conduction despite of doping ion and dose.

It can also be noticed that independently of the dose, Sb-doped samples show higher electrical resistivity than P-doped ones, indicating that in the latter the incorporation of doping ions into the ZnO lattice is more effectively achieved. For both series, resistivity decreases with increasing doping dose, since both type of carriers (n and p) contribute to resistivity.

Table II - Resistivity (ρ), carrier concentration (n_{Hall}) and Hall mobility (μ_{Hall}) of implanted ZnO samples

Sample	*Carrier type*	ρ (Ωcm)	n_{Hall} (cm^{-3})	μ_{Hall} $(cm^2V^{-1}s^{-1})$
ZnO:Sb1		0.146	5×10^{21}	10×10^{-3}
ZnO:Sb2	p-type	0.132	28×10^{21}	2×10^{-3}
ZnO:Sb3		0.042	7×10^{21}	20×10^{-3}
ZnO:P1		0.025	13×10^{21}	16×10^{-3}
ZnO:P2	p-type	0.015	38×10^{21}	11×10^{-3}
ZnO:P3		0.012	41×10^{21}	13×10^{-3}

In P-series the increase of the electrical conductivity with increasing dose is followed by the raise of carrier concentration, while Hall mobility keeps practically constant. This implies that the phosphorous ions effectively contribute to the p-type conductivity. The small difference between the results from films ZnO:P2 and ZnO:P3 suggest that the latter must be near doping saturation.

In Sb-series, samples ZnO:Sb1 and ZnO:Sb2 have an electric behaviour very similar to the P-doped ones. However, ZnO:Sb3 film has a quite different one: though its conductivity is higher than that of ZnO:Sb2, the Hall-effect-derived carrier concentration is lower, which suggests that the increase of the conductivity follows out an increase of n-type carriers, possibly resulting from a higher concentration of O-vacancies in this sample or from a poor incorporation of doping ions into it.

It should be noticed that the high value calculated for the Hall mobility in the ZnO:Sb3 film should not be directly associated to a high value of its mean free path, since it is consequence of the balance between the number of p-type and of n-type carriers.

Aiming to better understand the source of the difference between ZnO:Sb and ZnO:P resistivity values, as well as the peculiar number of carrier concentration obtained for ZnO:Sb3, Raman analysis have been performed.

Vibrational properties of the doped ZnO thin films have been studied by microRaman spectroscopy. Figure 2 and 3 show the Raman spectra of all samples. The characteristic 437 cm^{-1} peak of ZnO wurtzite structure, assigned to the non-polar optical phonons (E_2-high) mode is present in all spectra in a similar shape. Likewise, a broad band between 500 and 650 cm^{-1} is well defined in all of them, though its profile changes from P-doped films to Sb-doped ones. It is particularly intense in the latter and considerably differs for

different Sb-doping doses. The relation between this band and the E_2 peak increases from spectrum to spectrum as the Sb content rises, mainly from ZnO:Sb2 to ZnO:Sb3.
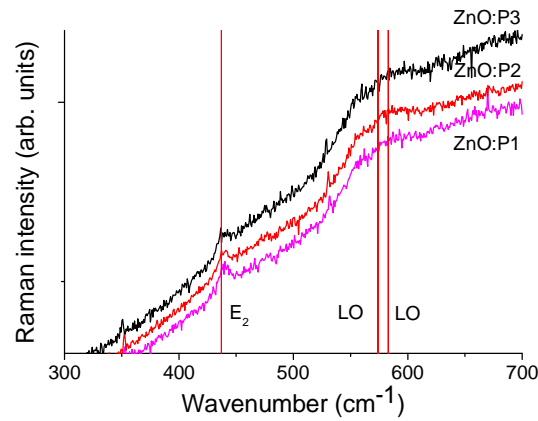

Figure 2 – Raman spectra of ZnO:P thin films excited with 488 nm laser line. The spectra intensity is vertically shifted for clarity.
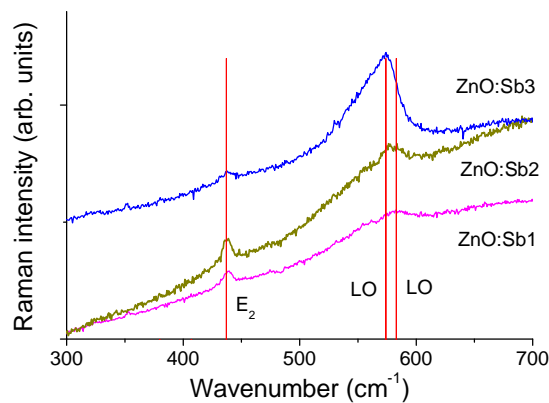

Figure 3 – Raman spectra of ZnO:Sb thin films excited with 488 nm laser line. The spectra intensity is vertically shifted for clarity.

According to literature, in this spectral range there are two phonon longitudinal (LO) modes of ZnO: at 574 cm^{-1} and at 583 cm^{-1} [12]. These modes are ascribed to defects of oxygen vacancies, interstitial Zn and free carriers [13, 14] . In our results another

Lonretzian contribution to the profile of this large band at around 555cm^{-1} must be considered. This peak has already been referenced in literature though its origin is not clear [15, 16].

A close look at the low frequency range denounces an extra asymmetric peak in the ZnO:Sb3 spectrum, not connectable to zinc oxide (Figure 4). Since the frequency of this peak (151 cm^{-1}) coincides with a bulk-Sb mode [17, 18] and its lineshape is strongly asymmetric, it can be associated to confined optical modes, to conclude the presence of an antimony nano-phase in this sample [19, 20]. Assuming the study of A. Roy et al, the presumed size of such nanoparticles is around 3 nm.
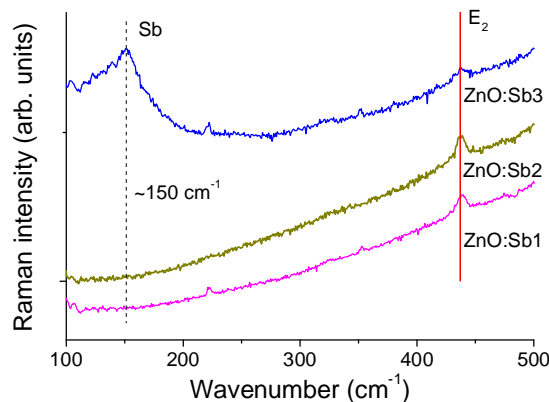

Figure 4 – Low frequency Raman spectra of ZnO:Sb thin films excited with 488 nm laser line. The spectra intensity is vertically shifted for clarity.

Thus, in ZnO:Sb3 a significant part of the doping ions have not effectively been incorporated in ZnO lattice, not contributing to the number of p-carriers. On the other hand, the number of n-carriers has considerably raise as it is evinced by the important increase of its related Raman phonon band (500 - 650 cm^{-1} band in figure 3). So, the net number of carriers, that contribute to the Hall charge concentration, is lower in ZnO:Sb3

than in ZnO:Sb2 film. Furthermore, the carrier addiction, that dictates conductivity, is more favorable in the former than in the latter and the resistivity of ZnO:Sb3 raises.

5. Conclusions

For all doping ions and doses we have obtained highly transparent films in the visible and IR regions having p conduction (p-ZnO). This means that for the doses and annealing temperature employed both Sb- and P-related acceptors are enough to prevail over the background electrons from natural ZnO. Furthermore, we are able to conclude that the P-doping is more efficient, since its incorporation into the lattice is less destructive and it is better disseminated within it, thus favouring larger carrier concentration and lower electric resistivity.

References

[1]   X.-L. Guo, J.-H. Choi, H. Tabata and T. Kawai, Jpn. J. Appl. Phys. 40, L177 (2001).

[2]   H. Cao, Y.G. Zhao, S.T. Ho, E.W. Seelig, Q.H. Wang and R.P.H. Chang, Phys. Rev. Lett. 82, 2278 (1999).

[3]   Zhang Xiaodan, Fan Hongbing, Zhao Ying, Sun Jian, Wei Changchun and Zhang Cunshan, Appl. Surface Science 253, 3825 (2007).

[4]   V.A. Coleman, H.H. Tan, C. Jagadish and S.O. Kucheyev, J. Zou, Appl. Phys. Lett. 87, 231912 (2005).

[5]   J. Lee, J. Metson, P.J. Evans, R. Kinsey and D. Bhattacharyya, Appl. Surface Science 253, 4317 (2007).

[6]   G. Rolo, J. Ayres de Campos, T. Viseu, T. de Lacerda-Arôso, M.F. Cerqueira, Superlattices and Microstructure in print (2007).

[7]   D.A. Minkov, J. Phys D: Appl. Phys. 22, 199 (1989).

[8]   L.J. Van der Pauw, Philips Research Reports 13, 1 (1958)

[9] Th. H. de Keijser, J.I. Langford, E.F. Mittemeyer, A.B.P. Rogels, J. Appl. Crystallogr. 11, 10 (1978).

[10] S. Maniv, W.D. Westwood, E. Coloboni, J. Vac. Sci. Technol. 20, 162 (1982).

[11] D.C. Look, Electrical Characterization of GaAs Materials and Devices, Wiley, New York, Chapter1 (1989).

[12] C. Bundesmann, N. Ashkenov, M. Schubert, D. Spemann, T. Butz, E. M. Kaidashev, M. Lorenz, and M. Grundmann, Appl. Phys. Lett. 83 (10), 1974 (2003)

[13] T.C. Damen, S.P.S. Porto, B. Tell, Phys. Rev. 142(2), 570 (1966).

[14] J.M. Calleja, M. Cardona, Phys. Rev. B 16, 3753 (1977).

[15] H.J. Fan, R. Scholz, F.M. Kolb, M. Zacharias, U. Gösele, F. Heyroth, C. Eisenschmidt, T. Hempel, and J.Christen, Appl. Phys. A 79, 1895 (2004).

[16] X.Q. Wei, B.Y. Man, M. Liu, C.S. Xue, H.Z. Zhuang and C. Yang, Physica B 388, 145 (2007).

[17] X. Wang, K. Kunc, I. Loa, U. Schwarz, and K. Syassen, Phys. Rev. B 74, 134305 (2006).

[18] H. Olijnyk, S. Nakano, and K. Takemuraphys, Stat. Sol. (b) 244 (10), 3572 (2007).

[19] A. Roy, M. Komatsu, K. Matsuishi, S. Onari, J. Phys. Chem Solids, 58 (5), 741 (1997).

[20] A. G. Rolo, M. I. Vasilevskiy, J. Raman Spectrosc. 38, 618 (2007).